26th AIAA Aerodynamic Measurement Technology and Ground Testing Conference AIAA Paper 2008-3710
June 23-26, 2008
Seattle, WA
SAND2008-3966C

The Influence of Velocity Gradients on PIV Measurements of Turbulence Statistics: A Preliminary Study

Steven J. Beresh*
Sandia National Laboratories, Albuquerque, NM, 87185

Error in Particle Image Velocimetry (PIV) interrogation due to velocity gradients in turbulent flows was studied for both classical and advanced algorithms. Classical algorithms are considered to be digital cross-correlation analysis including discrete window offsets and, for the present work, advanced algorithms are those using image deformation to compensate for velocity gradients. Synthetic PIV simulations revealed substantial negative biases in the turbulent stress for classical algorithms even for velocity gradients within recommended PIV design limits. This bias worsens if the distribution of velocity gradients has a nonzero mean, and error in the mean velocity may be introduced as well. Conversely, advanced algorithms do not exhibit this bias error if the velocity gradients are linear. Nonlinear velocity gradients increase the error in classical algorithms and a significant negative bias in the turbulent stress arises for the advanced algorithm as well. Two experimental data sets showed substantially lower turbulent stresses for the classical algorithm compared with the advanced algorithm, as predicted. No new experimental design rules for advanced algorithms are yet proposed, but any such recommendation would concern second-order velocity derivatives rather than first order.

Introduction

As Particle Image Velocimetry (PIV) processing algorithms have evolved, errors have declined from a once-accepted level of about one-tenth of a pixel to values as low as one-hundredth of a pixel [1, 2]. In particular, new algorithms better address errors associated with peak locking to integer pixel displacements and biases arising from large velocity gradients. These improvements can be attributed to the development of so-called advanced algorithms to replace older and simpler processing approaches that have become known as classical algorithms.

Classical algorithms generally are considered to be digital implementations of the cross-correlation-based analysis discussed by Keane and Adrian [3], as first credited to Willert and Gharib [4]. Usually, this class of algorithms additionally incorporates discrete window offsets in which a first pass through the images determines the integer value of the local particle displacement, then a second pass shifts each interrogation window by that amount to minimize in-plane particle loss [5]. Advanced algorithms cover a multitude of additions to a classical processing technique. These would include such enhancements as iterative grid refinement for improved spatial resolution and dynamic range [6], image deformation for the treatment of velocity gradients [1], self-calibration to correct stereoscopic misalignment [7], Hart's correlation-based corrections [8], or optical flow image analysis [9]. This list hardly can be considered comprehensive and does not even include the many developments related to PIV applications in micro-flows. For the purposes of the present paper, the term "advanced algorithms" is meant to encompass those that commonly have been implemented in commercial PIV software and have found widespread use; principally, this refers to image deformation and iterative grid reduction.

The practical differences between classical and advanced algorithms became apparent to the present author in a recent comparison of data originally processed using a classical algorithm and then later revisited with an advanced algorithm [10]. Although mean velocities agreed to within the uncertainty, substantial biases towards lower values were found in the turbulent stresses computed by classical PIV software as compared to the newer software

*Principal Member of the Technical Staff, Engineering Sciences Center, Senior Member AIAA, correspondence to: P.O. Box 5800, Mailstop 0825, (505) 844-4618, email: sjberes@sandia.gov

This paper is declared a work of the U.S. Government and is not subject to copyright protection in the United States.

This work is supported by Sandia National Laboratories and the United States Department of Energy. Sandia is a multiprogram laboratory operated by Sandia Corporation, a Lockheed Martin Company, for the United States Department of Energy's National Nuclear Security Administration under Contract DE-AC04-94AL85000.

implementing advanced algorithms. Whereas past studies have shown the efficacy of the image deformation algorithm in extracting valid velocity vectors from regions of high velocity gradients in which classical PIV algorithms fail [11-13], these new results demonstrated that even where velocity vectors may be computed successfully by classical PIV, substantial bias errors may still occur. Furthermore, these bias errors in turbulence measurements are found even for velocity gradients that lie within the recommended limits for classical PIV.

The errors located in Ref. [10] have prompted a closer examination of the accuracy of turbulence data processed prior to the availability of advanced algorithms, and the error that may remain even with advanced algorithms. Although some studies discuss differences in bias errors between classical and advanced algorithms [11, 14-16], none of these reports explicitly analyzes turbulence quantities. The present work uses synthetic PIV images to examine exactly this question and apply the results to two experimental turbulent data sets.

Background

As PIV has become one of the most widely used modern diagnostics in fluid dynamics, development and analysis of new interrogation algorithms has received widespread attention and, consequently, numerous publications. Though the sheer quantity of reported improvements can be daunting for the non-specialist, Adrian's 2005 review [17] finds that "we are closing in on algorithms that are near optimum" and the series of PIV Challenges has been suspended since 2005 due to a reduction in the pace of interrogation improvements [18].

The most important of the advanced algorithms in the context of the present study is image deformation, or alternatively, window deformation. The distinction is merely that image deformation warps an entire PIV image based upon estimated displacements and velocity gradients, whereas window deformation proceeds by warping individual interrogation windows independently. Huang *et al*. [12] were first to mitigate the damaging effects of velocity gradients upon a correlation pattern by warping interrogation windows, but computer performance of that day made computation time impractically lengthy. As computer technology rapidly developed and image deformation algorithms matured (for example, Fincham and Delerce [14] or Scarano and Reithmuller [11]), the technique not only became feasible, but in fact proliferated into most modern PIV processing software.

When Huang *et al*. [12] first introduced image deformation, they found its chief benefit to be its ability to extract valid velocity vectors from regions of high velocity gradient in which classical PIV algorithms fail. Subsequent studies utilizing more developed forms of the algorithm concurred with this assessment [11, 13], but improvements in measurement accuracy were discovered as well. The peak-locking errors that commonly plague classical PIV algorithms (in which measured displacements tend to cluster around integer pixel values) are dramatically reduced by image deformation algorithms [1, 11, 14, 19]. This is not a result of improved sub-pixel precision, although image deformation does help in this regard [1, 11, 14, 19], but because classical algorithms filter out relevant velocity information that image deformation successfully retrieves [11-13]. Random errors have been shown to diminish with image deformation as well [11, 14, 15].

Different sorts of errors in PIV interrogation arise due to velocity gradients. The additional correlation noise due to velocity gradients has been recognized since the infancy of PIV [20] and is caused by the simultaneous broadening of the correlation peak and the reduction of its amplitude as non-identical particle displacements are summed within an interrogation window. Bias errors can be even more pernicious and arise from at least two sources: Westerweel [21] describes the mathematical bias towards zero displacement that occurs due to the skewing of the correlation peak when employing cyclic FFT algorithms for cross-correlations, as is most often the case in PIV analysis; this phenomenon grows more severe as velocity gradients broaden the peak. Lecuona et al. [13] discusses the group-locking phenomenon, in which velocity gradients that vary within an interrogation window introduce an additional bias. These errors are inherent in classical PIV algorithms, but numerous studies have demonstrated the advantages of image deformation in the analysis of flows with strong velocity gradients [1, 2, 11-13, 15], which is one of the reasons why it has become prevalent in PIV processing.

The cumulative effect of PIV interrogation errors upon turbulent quantities has been considered by several studies, though of course any approach that reduces interrogation error is expected to be reflected in turbulence measurement. Christensen [22] has demonstrated that peak locking can seriously bias measurement of turbulent fluctuations even while having no discernable impact upon the mean, but that this degree of peak locking is unlikely even for classical PIV algorithms provided a reliable Gaussian estimator is used for correlation peak estimation. For advanced algorithms incorporating image deformation, significant error in turbulence statistics due to peak locking is unlikely. However, as noted earlier, other sorts of bias errors are present in PIV interrogation as well, which may impact turbulence measurements. Piirto *et al*. [19] found improved agreement in turbulence quantities with a direct Navier-Stokes simulation for some cases when using image deformation, but data were not universally improved by this algorithm. Similarly, the second PIV Challenge [2] found improved turbulence measurements using image

deformation when images possessed a near-optimal particle image diameter, particularly where the velocity gradient was strong, but other factors were dominant for smaller particle images. Indeed, mixed results in turbulence data when employing image deformation may be attributable to the particle image size relative to the pixel size; Astarita and Cardone [23] find insufficient information for a meaningful interpolation between pixels when the particle image diameter approaches a single pixel, and in this case image deformation is not useful; Kim and Sung [24] also find greater error for particle image diameters near one pixel.

Conducting a successful turbulent PIV experiment continues to rely upon design rules dating from PIV's infancy. Keane and Adrian's [3] classical analysis recommends a maximum allowable pixel displacement due to the velocity gradient of no more than 3% of the interrogation window width; that is, $M|\Delta u|\Delta t/d_I<0.03$ where M is the magnification, Δu is the difference in velocity across an interrogation window, Δt is the time between laser pulses, and d_I is the size of the interrogation window. More simply, this may be expressed as $|\Delta u|/d_I<0.03$, where both Δu and d_I are now expressed in pixels. However, this analysis was based upon detection probability and does not consider potential for error even for successful correlation peak detection. Westerweel [21] provides a more specific guideline, also for classical PIV, that the velocity gradient not exceed the ratio of the particle image diameter to the interrogation window width, that is, $|\Delta u|<d_p/d_I$, which he notes is ordinarily about 3-5% and hence consistent with Keane and Adrian [3]. Lecuona *et al*. [13] recognize that the maturation of PIV has led to application in more demanding flowfields and in fact advanced processing algorithms such as image deformation allow Keane and Adrian's criteria to be exceeded; the second PIV challenge demonstrated this as well [2]. No updated design rules for advanced algorithms are known to the present author.

Experimental Apparatus

Differences in the measurement of turbulent statistics by advanced PIV algorithms as compared to classical algorithms are investigated using two different experimental data sets as well as through the use of synthetic PIV data. The first experiment concerns a supersonic jet in subsonic compressible crossflow and has previously been published elsewhere [25, 26] including a recent detailed examination of the uncertainties [10]. A second data set was gathered in the wind tunnel wall boundary layer but has not seen prior publication.

Common Hardware

Both experiments were performed in Sandia's Trisonic Wind Tunnel (TWT), which is a blowdown-to-atmosphere facility using air as the test gas through the facility's 305 × 305 mm^2 solid-wall transonic test section enclosed within a pressurized plenum. The TWT is seeded by a thermal smoke generator (Corona Vi-Count 5000) that produces a large quantity of particles typically 0.2 - 0.3 μm in diameter from a mineral oil base, delivered to the TWT's stagnation chamber upstream of the flow conditioning section.

PIV measurements were two-component (2-C) for the jet-in-crossflow experiment and stereoscopic (3-C) for the boundary layer experiment, acquired with the laser sheet aligned in the streamwise direction of the wind tunnel on the test section centerline, as shown in Fig. 1. The coordinate system is chosen such that the u component lies in the streamwise direction and the v component is in the vertical direction, positive away from the top wall; the origin is located at the center point of the jet nozzle exit plane (see below).

The light source for PIV measurements was a pair of frequency-doubled Nd:YAG lasers (Coherent Infinity 40-100) for the jet-in-crossflow experiment and a dual-cavity Nd:YAG laser for the boundary layer experiment (Spectra Physics PIV-400). Scattered laser light was collected by interline-transfer CCD cameras (Redlake MegaPlus ES4.0/E) with a resolution of 2048 × 2048 pixels digitized at 8 bits. For the 2-C streamwise measurements, a single camera was equipped with a 105 mm lens (Nikon Micro-Nikkor) operating at f/4 and standing 1.1 m from the laser sheet. Calibrations of the 2-C PIV data were accomplished simply by imaging a target placed in the measurement region to convert the object plane length scale to the image plane length scale. Stereoscopic PIV used two cameras equipped with 105 mm lenses mounted on Scheimpflug platforms to create an oblique focal plane aligned with the laser sheet. Camera calibrations have been performed using a multi-plane procedure.

Jet-in-Crossflow Experiment

A jet nozzle with a design Mach number of 3.73 was mounted along the centerline of the top wall of the test section well upstream of the PIV measurement location, as seen in Fig. 1, to acquire data in the far-field of the interaction. The jet used a nitrogen supply and exhausted from a conical nozzle with an expansion half-angle of 15° and an exit diameter d_j of 9.53 mm. Data considered in the present paper have a freestream Mach number M_∞=0.8 with a wind tunnel stagnation pressure P_0=154 kPa. The jet stagnation pressure was varied to produce four different values of the jet-to-freestream dynamic pressure ratio J to examine the impact of varying the relative strength of the

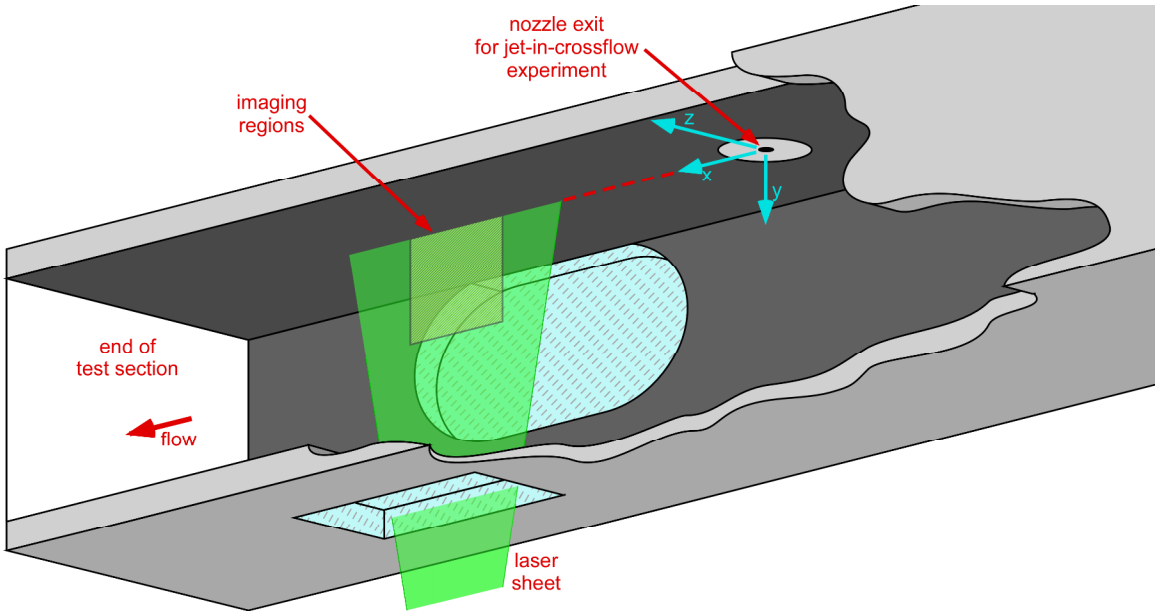

Fig. 1: A schematic of the laser configuration in the wind tunnel for PIV measurements in the streamwise plane, looking from below the test section in the downstream direction. Flow is from right to left. All dimensions are in millimeters. Not to scale.

jet, but P_{0j} was chosen such that the jet was always overexpanded.

For this experiment, the PIV system was configured to provide a laser sheet thickness of 1.2 mm and a pulse separation time of 2.375 μs. The field of view of the camera measured approximately 160 × 160 mm^2. Sufficient data for reasonable convergence of turbulence quantities were acquired in all cases, though many more image pairs were collected for J=10.2: about 3000, as compared to about 1000 for the other values of J.

Transonic Boundary Layer Experiment

The PIV system was reconfigured to measure the boundary layer on the same wall of the wind tunnel from which the jet emerges, but with the jet replaced by a blank. The measurement plane was aligned to approximately the same position as the jet-in-crossflow experiment and the field of view reduced to about 45 mm vertically rather than the 150 mm used for the jet-on data. Here, stereoscopic PIV was employed. The near-wall measurement capability was improved by inserting an anti-reflective coated exit window for the laser sheet into the top wall of the wind tunnel. Data were acquired at several freestream Mach numbers, all with a static pressure of p_w=101 kPa. Ten wind tunnel runs, each of 150 image pairs from each camera, were conducted for each Mach number.

Particle Image Velocimetry Software

Data from both experiments initially were processed using IDT's ProVision 2.02, which employs a classical PIV algorithm. A later purchase of LaVision's DaVis 7.1 allowed reprocessing of the same images using advanced algorithms incorporated into the software, chiefly featuring image deformation based upon local velocity gradients using a bilinear interpolation scheme to warp the images. Regardless of the software, the jet-in-crossflow image pairs were interrogated with a 64 × 64 pixel window employing two iterations with adaptive window offsets to account for the local particle displacement. The relatively large interrogation window was chosen to favor precision over spatial resolution, needed for the relatively small particle image diameter that results as a combination of the need for accurate particle response, a large field of view, and weak light intensity in side-scatter mode. The smaller field of view and increased laser power for the boundary layer experiment was more successful with smaller interrogation windows; therefore 32 × 32 pixel windows were used, again with two iterations. An approximate 50% overlap in the interrogation windows was typically used as well to oversample the velocity fields in all cases. The resulting vector fields were validated based upon signal-to-noise ratio and nearest-neighbor comparisons.

Synthetic PIV

To examine the performance differences between the IDT (classical algorithm) and LaVision (advanced

algorithm) software, the well-established tactic of synthetic PIV images was employed. Sets of 1000 image pairs of 256 × 256 pixels each were generated for 2-C analysis, but velocimetry results were obtained only for the interior of the images such that no edge effects occurred. Particle images were created with a Gaussian intensity distribution of fixed width and particle locations were randomly chosen centered at subpixel values. Various particle diameters and seeding densities were tested to represent different seeding conditions. Shown in this document are three cases: a particle image diameter of $d_p \approx 3$ pixels seeded at a mean density of ten particle pairs per 64 × 64 interrogation window with image saturation at half the maximum particle intensity; $d_p \approx 1.5$ pixels with a much higher seeding density and no saturation except when particle images overlap; and $d_p \approx 1.0$ pixels at similar conditions. The real PIV data that are the focus of this paper lie somewhere between the latter two cases, with the boundary layer experiment producing particle images closer to $d_p \approx 1.5$ pixels. Other particle sizes and seeding parameters were examined and the results found consistent with the forthcoming conclusions. One-dimensional turbulence was simulated by assigning a streamwise displacement to each image pair, varying with streamwise distance according to several different schemes as discussed below, then the correct velocities were recorded for later comparison with the PIV analysis.

Results and Discussion

Synthetic PIV

To establish a baseline for the performance of the two PIV algorithms, synthetic PIV images first were created for uniform flow by assigning a unique, non-integer streamwise displacement to each image pair, such that every particle in that image pair possessed the identical displacement. Displacements were randomly chosen for each image pair using a Gaussian distribution of some assigned width σ_v, whose magnitude establishes the simulated turbulent intensity, then the correct velocities were recorded for later comparison with the PIV analysis.

The results of processing the synthetic PIV images with both the IDT and LaVision software are shown in Fig. 2, where Fig. 2a displays the error in the mean over the 1000-image-pair set (the mean is nominally zero, but not precisely) and Fig. 2b gives the error in the streamwise turbulent stress. Neither the mean nor the turbulent stress displays error that is a meaningful function of the simulated turbulent strength. Only the $d_p \approx 3$ data as processed by IDT shows much variation with σ_v, and this is probably convergence error for the mean and additional noise in the turbulent stress due to difficulty in locating the correlation peak for a large, saturated particle image [21, 27]. The LaVision software returns significantly better results for these relatively large particle images, which can be attributed to its use of image deformation (which for uniform flow is equivalent to sub-pixel window offsets), though this case still produces a larger error in the turbulent stress than any other LaVision result. Excepting the $d_p \approx 3$ case, which is not the best representation of the real data in this study, the errors in the mean velocity are less than 0.001 pixel and in the turbulent stress less than 0.01 pixel, which are negligibly small.

Velocity gradients must be added to the synthetic PIV to seek meaningful differences in the performance of the two software packages, which was accomplished by modifying the simulated one-dimensional turbulence to include an additional parameter σ_g, which describes the width of a Gaussian distribution of velocity gradient strength. For each image pair, the velocity strength first is randomly selected based upon σ_v, same as previously, but then a linear gradient across the image is imposed whose magnitude is randomly chosen using σ_g in an identical fashion to the selection of the velocity magnitude. Figure 3 shows the results from each software package as a function of σ_g when

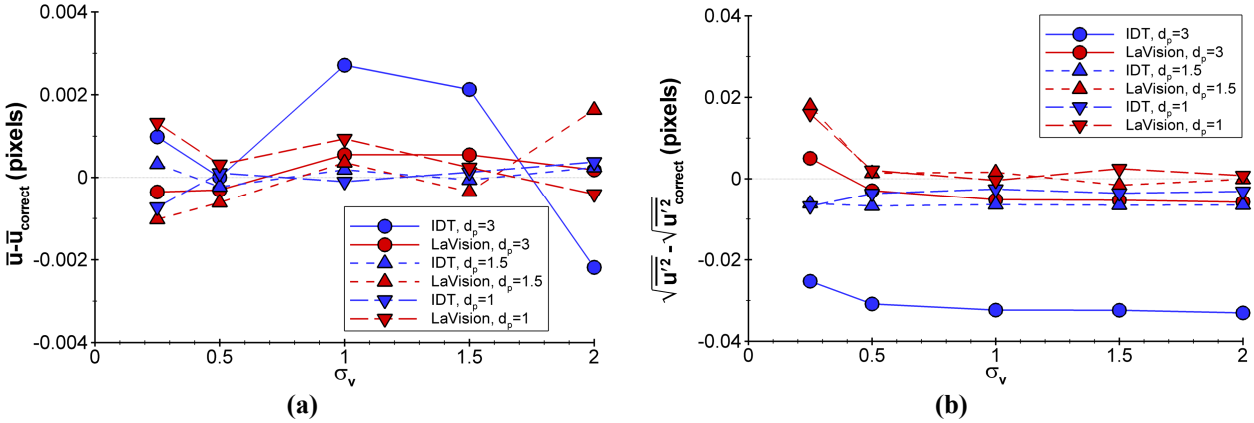

Fig. 2: Error in synthetic PIV images of one-dimensional turbulence as processed by IDT or LaVision software as a function of the simulated turbulent intensity. (a) mean velocity; (b) turbulent stress.

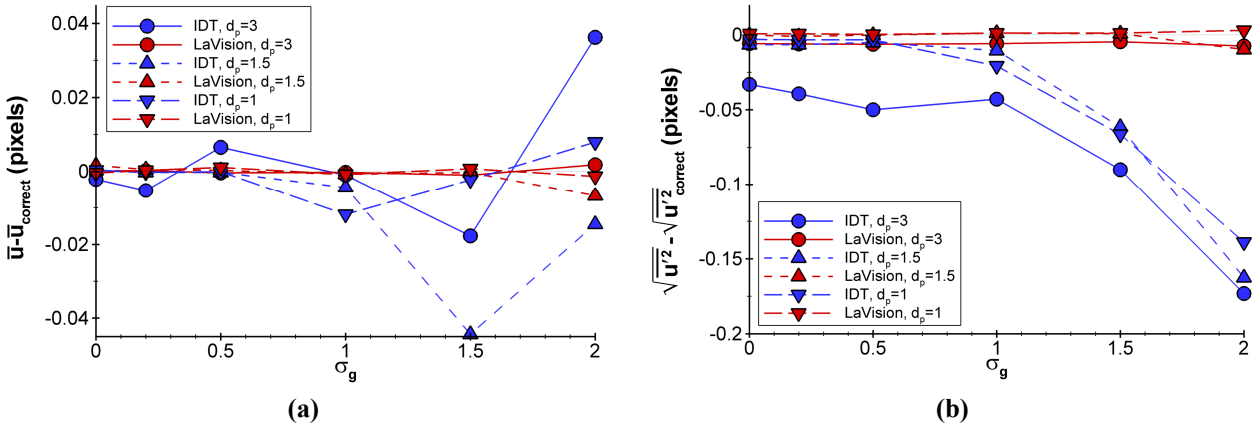

Fig. 3: Error in synthetic PIV images with an imposed linear velocity gradient as a function of the magnitude of the simulated gradient distribution (σ_v =2.0). (a) mean velocity; (b) turbulent stress.

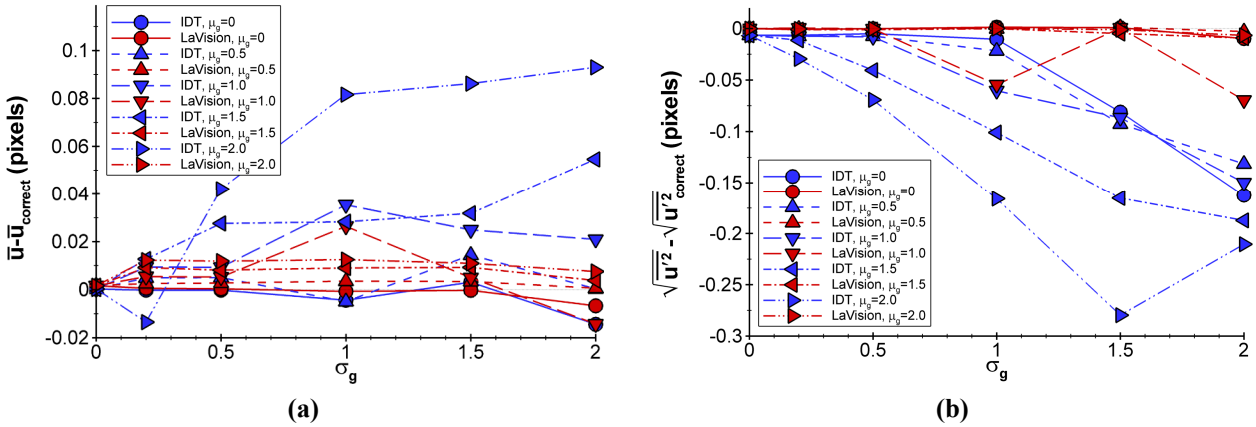

Fig. 4: Error in synthetic PIV images with linear velocity gradients chosen from a Gaussian distribution of mean μ_g and width σ_g (σ_v =2.0, d_p=1.5). (a) mean velocity; (b) turbulent stress.

σ_v is fixed at 2.0, displaying a clear, significant difference in the turbulent intensity error for the two analyses. The mean error is very small and invariable with respect to σ_g for the LaVision results, but the IDT data become more erratic as the gradient strength rises, probably as a result of convergence error for increasingly noisy results. The error in the turbulent stress is particularly revealing; again, the error in the LaVision results is low and constant, but here the error in the IDT results increases markedly as the gradient becomes stronger and reaches a magnitude of nearly 0.2 pixels, a substantial measurement bias. The bias direction is negative, displaying a reduced turbulent stress for the classical algorithm as compared to the advanced algorithm.

It is interesting to further note that Fig. 3 indicates that the LaVision results are not a significant function of the particle image diameter, even though Astarita and Cardone [23] show that most subpixel interpolation schemes return error levels of about 0.1 pix as d_p becomes small enough. It therefore would be anticipated that particles of about d_p=1 do not provide sufficient information for a meaningful interpolation between pixels and in this case image deformation is not useful, as in case A of the Second PIV Challenge [2]. In the present case, both for the synthetic PIV and the real data presented later, the particle density is quite large and particle images commonly overlap. This creates structures in the images with characteristic lengths exceeding a single pixel, and therefore larger values for the corresponding size of the patterns upon which the software correlates.

The simulated turbulence of Fig. 3 assumes that the velocity gradients will occur randomly in either streamwise direction with a mean of zero, but many turbulent flows exhibit velocity gradients in a single known direction, or, even accounting for the randomness of turbulence, have velocity gradients preferential towards one direction or the other. To add this factor into the synthetic PIV, the mean of the Gaussian distribution from which σ_g is extracted was shifted by a fixed amount in the positive direction. Figure 4 shows these results, with σ_g chosen as previously and σ_v =2.0, and the curves differentiated based upon the mean of the gradient distribution μ_g. To simplify the

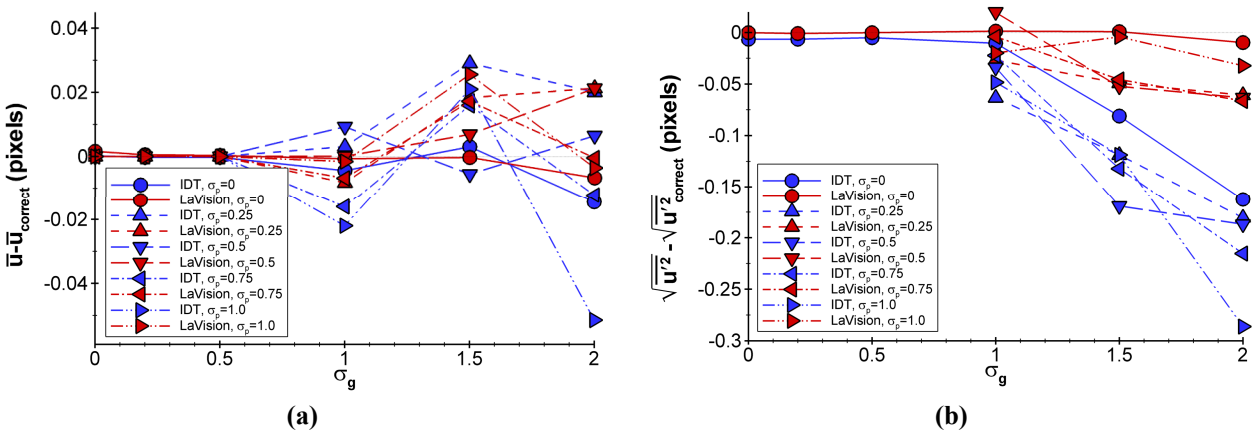

Fig. 5: Error in synthetic PIV images with an imposed linear velocity gradient of power-law rather than linear character (σ_v =2.0, d_p=1.5). (a) mean velocity; (b) turbulent stress.

analysis, only d_p≈1.5 was considered because results in Figs. 2 and 3 did not shown meaningful differences due to the particle image diameter.

The turbulent stress results in Fig. 4b behave as would be anticipated from the earlier results of Fig. 3b. As the mean μ_g is shifted towards larger positive values, clearly more large gradients will be generated and fewer small ones, and hence the bias error in the classical algorithm increases in accordance with the trend of Fig. 3b. The error in the advanced algorithm of the LaVision software remains near zero, rising to about 0.01 pixels in the worst case (excepting the μ_g=1.0 case, which is probably an anomaly). More interesting are the mean velocity results in Fig. 4a, in which substantial bias errors arise in the IDT results as μ_g is increased. This bias can reach a level as high as 0.1 pixel, equivalent to the generally accepted error level of classical algorithms and therefore a significant addition to the total error of the measurement. Even the LaVision results show an increase in the bias error, to a level of about 0.01 pixel. Because the imposed velocity gradient remains linear for this test case, the group locking phenomenon of Lecuona *et al*. [13] cannot account for it. Similarly, Westerweel [21] demonstrated that the insufficiency of the view that lower velocities will be more strongly represented because faster particles are more likely to leave the interrogation window, and furthermore, the use of window offsets introduces the possibility that the smallest particle displacements will be left out of a shifted interrogation window.

Additional biases can be expected when the velocity gradient does not simply vary linearly across an interrogation window [1, 12, 13, 15]. This influence was investigated by imposing a velocity gradient of power-law rather than linear character, that is, u=Ax^C rather than u=Ax as previously. The exponential constant C is always positive and is randomly chosen for each image pair from a one-sided Gaussian distribution of width σ_c. Results are given in Fig. 5, again only for d_p≈1.5 and σ_v =2.0, and always with μ_g =0. Simulations were not run for σ_g=0.2 and 0.5, but this does not restrict interpretation of the results. The erratic behavior of the mean error in Fig. 5b, for both software packages, exhibits the characteristics of increased convergence error as another random parameter has been added. Figure 5b shows increased error in the turbulent stress as additional nonlinear character is introduced to the velocity gradients, and that this rise in bias error occurs for both the classical algorithm of IDT and the advanced algorithm of LaVision. In the worst case, the IDT error nearly doubles to 0.3 pixels, but the LaVision error rises from essentially zero to about 0.07 pixels. Moreover, it appears that the LaVision error is somewhat constant with the order of the gradient curvature and even with the gradient strength, suggesting that image deformation quickly acquires significant error levels as soon as the assumption of linear velocity gradients is violated.

Jet in Crossflow

Results of the jet-in-crossflow experiment have been thoroughly documented in Refs. [25, 26]. Here, just the vertical velocity component will be examined because this is the strongest component in both the mean and the fluctuations. Figure 6a shows the mean vertical velocity profiles for each of four values of J, whereas Fig. 6b provides the equivalent vertical component of the turbulent stress. The error bars are taken from the uncertainty analysis found in Ref. [25] or Ref. [10], and it is clear that the mean velocities agree to well within the uncertainty, whereas the turbulent stress shows a significant discrepancy attributable to the difference in PIV interrogation algorithm. However, the given error bars for the mean measurements include calibration biases that are crucial when considering the probable correct value of a measurement, but will cancel when simply comparing between

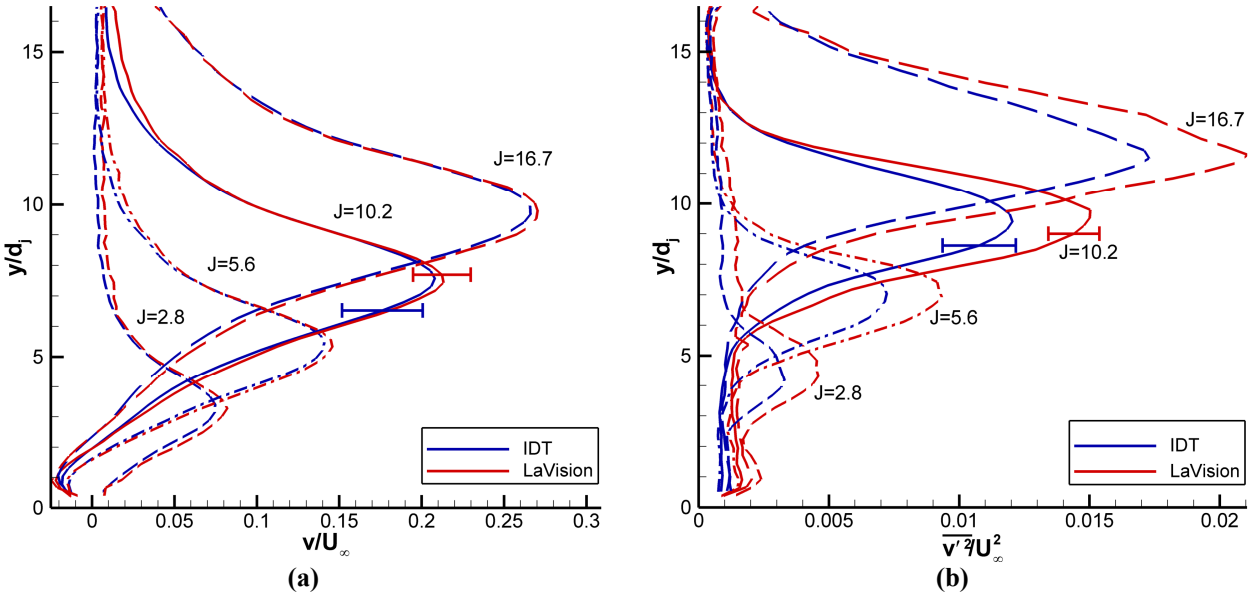

Fig. 6: Vertical velocity component of the jet-in-crossflow measurements at x/d_j=33.8 downstream of the jet. (a) mean velocity; (b) turbulent stress.

interrogation algorithms; when removing this component of the uncertainty, the error bars of Fig. 6a drop to nearly half the size (about 0.01 U_∞) but those of Fig. 6b are essentially unchanged.

Next, it is necessary to determine if the gradients found in the jet-in-crossflow data are sufficiently large to generate errors consistent with Fig. 3. The maximum mean velocity gradient for J=10.2 in Fig. 6a is 1800 s^{-1}, which equates to 0.4% of d_I and is well within Keane and Adrian's PIV design recommendation. Of course, the PIV software does not correlate on the mean flowfield but on instantaneous realizations of it, so the actual velocity gradients to which the algorithms are subjected must be determined *a posteriori* from the PIV vector fields themselves. Figure 7 shows a sample instantaneous vector plot of the velocity fluctuations, from which numerous individual turbulent eddies may be seen. The velocity gradient dv/dy was computed and is shown as a superposed contour plot; this derivative is somewhat larger than the other three in-plane components and hence is used for analysis. All recorded values of dv/dy were histogrammed over the entire data set at a single point in the flow corresponding to the peak of the turbulent stress curves in Fig. 6b and the resulting distribution of possible values of this derivative is given in Fig. 8, expressed in terms of $M|\Delta u|\Delta t/d_I$. Also plotted in Fig. 8 are distributions of the velocity gradients in the synthetic PIV simulations for varying σ_g with constant σ_v=2.0 and d_p=1.5, i.e., the gradient distributions corresponding to the d_p=1.5 curve of Fig. 3.

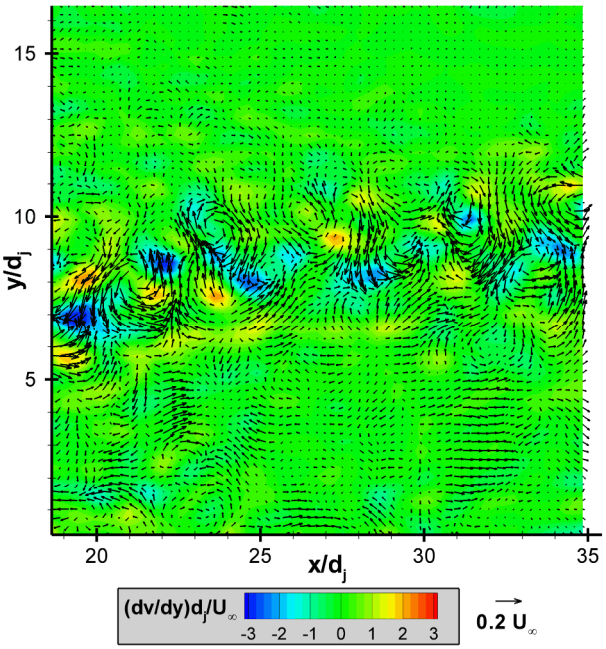

Fig. 7: Instantaneous realization of the velocity fluctuation field for the jet-in-crossflow experiment at J=10.2 overlaid on one component of the derived velocity gradient.

The first feature to notice in Fig. 8 is that the maximum velocity gradient in the flow is actually about 3% of d_I, considerably greater than the value found from the mean velocity profile. The distributions are approximately symmetric about zero. It also is evident that none of the synthetic PIV profiles quite match the shape of the actual data, which indicates that the approach taken to simulating turbulence bears improvement. Nonetheless, the jet-in-

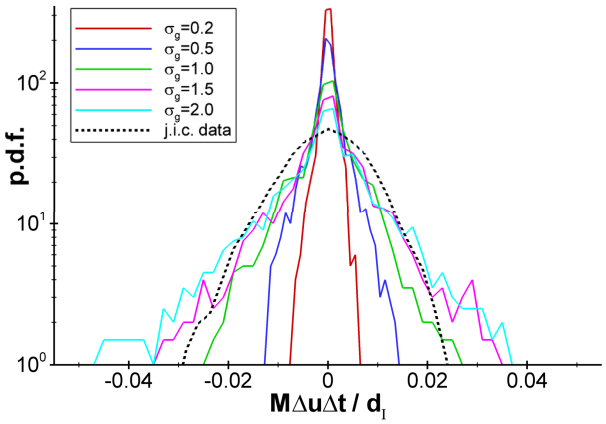

Fig. 8: Distribution of instantaneous velocity gradients dv/dy in the jet-in-crossflow data. Also shown are the distributions from the synthetic PIV (σ_v=2.0 and d_p=1.5).

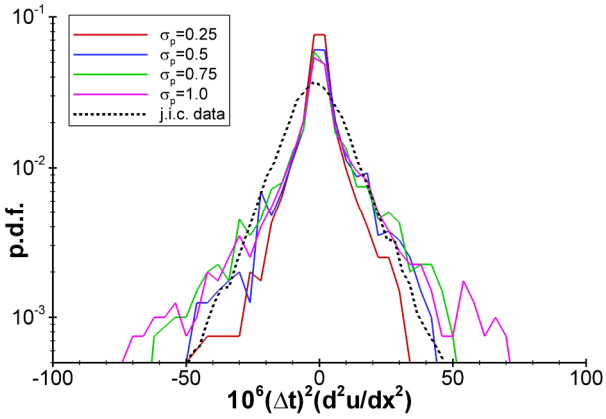

Fig. 9: Distribution of instantaneous second-order velocity gradients in the jet-in-crossflow data. Also shown are the distributions from the synthetic PIV (σ_v=2.0, σ_g=2.0, and d_p=1.5).

crossflow distribution is a reasonable correspondence to the σ_g=1.5 or 2.0 simulations. Referring to Fig. 3b, that suggests a bias error in the turbulent stress of about 0.1 to 0.15 pixels when using classical algorithms. For the configuration of the jet-in-crossflow experiment, that translates to about 3 – 5 m/s, a value of the same order as the estimated measurement uncertainty. In fact, reducing the velocity fluctuations in Fig. 6b measured using the LaVision software by this amount produces the magnitudes returned by the IDT software, so the unaccounted error in the turbulent stress may be fully attributed to the bias errors found in classical algorithms. The velocity gradients in the jet-in-crossflow data reach a maximum level of 3% of the interrogation window width, and usually are quite less, which satisfies the recommendation of Keane and Adrian [3]. Nevertheless, it is clear that whereas the error in the mean velocity measurement is insignificant, the error in the turbulent stress is unmistakably large.

The largest second derivatives in the jet-in-crossflow data are found to be the d^2v/dx^2 component, which may be examined similarly to the velocity gradients. Figure 9 shows the distribution of the velocity second derivative computed at the same point in the data as the gradients in Fig. 8, superposed on the equivalent distributions from the synthetic PIV of Fig. 5 for varying σ_p with constant σ_v=2.0 and σ_g=2.0. Again, the synthetic PIV profiles are an inexact match to the actual data, but nevertheless, reasonable inferences may be drawn. Clearly, the jet-in-crossflow measurements have a range of second-order velocity gradients similar to those in the synthetic PIV for σ_p between 0.5 and 1.0, which Fig. 5 indicates will lead to an additional negative bias error in the turbulent stress of approximately 0.05 pixels. This is true of both classical and advanced algorithms, which suggests that some significant error remains in the measurement of turbulent stresses even when employing image deformation to account for the velocity gradients, at least for the implementation in the LaVision software.

Transonic Boundary Layer

The preceding analysis for the jet-in-crossflow data was repeated for the transonic boundary layer experiment. Only the M_∞=0.8 data are presented in the interest of providing clearer figures, but similar results were found in data ranging from M_∞=0.5 to 0.85. The streamwise component is given in Fig. 10, with Fig. 10a providing the mean velocities from both the IDT and LaVision interrogation and Fig. 10b showing the corresponding turbulent stress. The uncertainty estimates are dominated by precision error because the biases mostly cancel out when examining normalized data, which reduces the error bars such that even the small difference between the two curves may be viewed as borderline significant. Conversely, the difference between the turbulent stress curves in Fig. 10b unequivocally is significant. Clearly, the IDT results have an additional issue with near-wall interrogation; despite the low-intensity laser reflection owing to the AR-coated exit window, the LaVision software appears to offer superior performance in this regard. However, as will be seen momentarily, this may not be solely due to laser flare.

As in the jet-in-crossflow analysis, the velocity gradients with which the PIV software must cope were examined by histogramming the instantaneous gradients found *a posteriori* in the vector fields, though here du/dy was used because it is the strongest component of the velocity gradient. Rather than recording all gradients at a single point throughout the entire data set, gradients were determined from a sample of vector fields over regions of the boundary layer. The results are given in Fig. 11 along with velocity gradients from the synthetic PIV

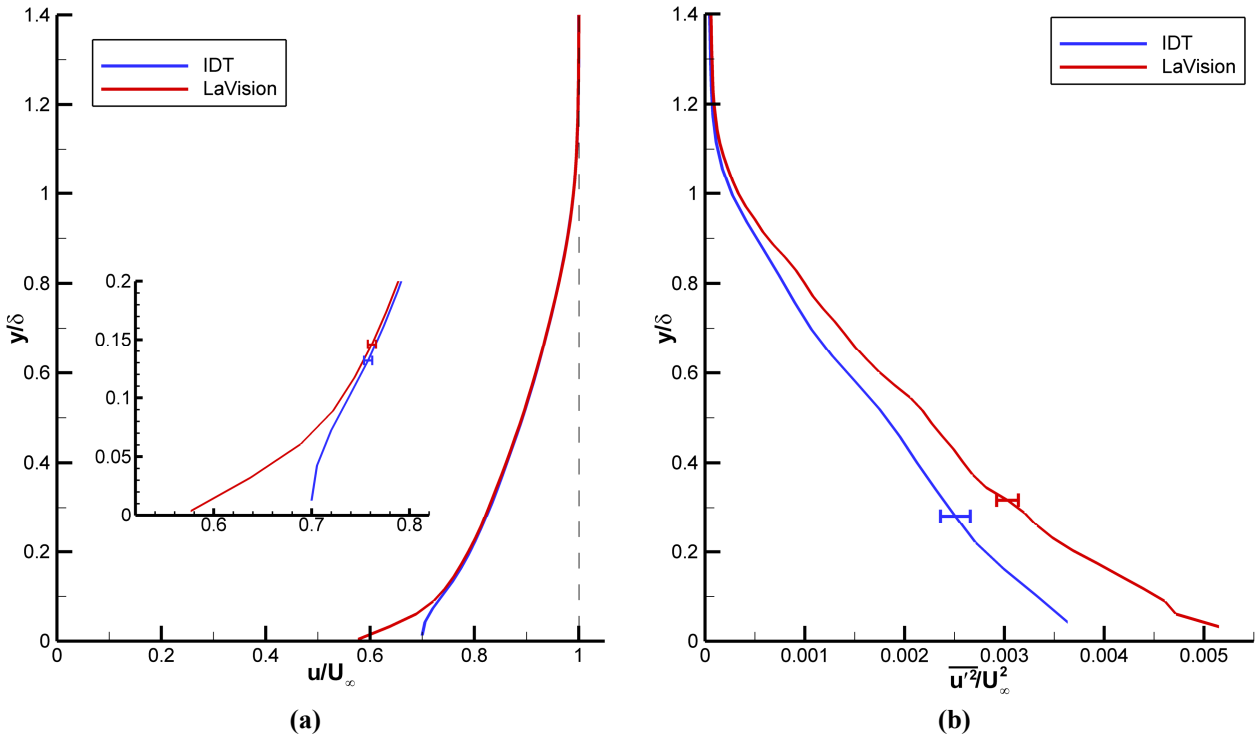

Fig. 10: Streamwise velocity component of the transonic boundary layer measurements at M_∞=0.8. (a) mean velocity; (b) turbulent stress.

simulations for varying μ_g with constant σ_g=2.0, σ_v=2.0, and d_p=1.5; i.e., the gradient distributions corresponding to the σ_g=2.0 data points of Fig. 4. First examining the distributions from the boundary layer data, it is evident that the curves are asymmetrical, with a substantially greater probability of finding positive gradients in the flow than negative. As gradients are gathered from a narrower portion of the boundary layer nearer to the wall, the distribution asymmetry increases, they become broader, and their peaks shift from zero to a positive value. The magnitude of the positive velocity gradients often is well past the recommended 3% limit, and the difficulty becomes more acute closer to the wall.

Consistent with the earlier jet-in-crossflow velocity gradient distributions, none of the synthetic PIV distributions exactly matches the real data, but sufficient agreement exists to permit some insight. The synthetic PIV curves do not exhibit a Gaussian shape because of the interplay between the velocity magnitude and the velocity gradient distributions. The μ_g=1.5 or μ_g=2.0 curves can be considered a reasonable approximation for the boundary layer data. Consulting Fig. 4, the synthetic PIV predicts a positive bias error in the mean velocity of almost 0.1 pixel in the IDT results and 0.01 pixel in the LaVision results. Figure 10a indeed shows the IDT velocity profile slightly larger than the LaVision profile. A bias error of 0.1 pixel corresponds to about 2 m/s for the PIV configuration of this experiment, or about $0.007U_\infty$. The difference between the two profiles at a height of y/δ=0.2 is $0.003U_\infty$, but these error values are so small it becomes very difficult to distinguish one sort of potential measurement error from the many others that will plague an experiment. However, extrapolating from the available simulations, as data are acquired closer to the wall and the velocity gradient distribution becomes more skewed towards positive values, Fig. 4a suggests that the IDT error will continue to increase whereas the LaVision error will remain fairly constant. This behavior would be consistent with the rapidly increasing error exhibited by the IDT results near the wall, so it is conceivable that correlation error due to laser flare from the wall is not solely responsible.

Regarding the turbulent stress profile in Fig. 10b, the simulations of Fig. 4b suggest a negative bias error in the IDT profile of perhaps 0.2 to 0.25 pixel and a probably negligible error in the LaVision profile. This corresponds to roughly 4 m/s, which works out to about twice as much error as is actually seen in Fig. 4b. It is not presently clear why the synthetic PIV appears less representative of the turbulent stress bias error in the boundary layer experiment than it was for the jet-in-crossflow experiment; more representative simulations than those seen in Fig. 11 will need to be conducted before conclusions may be drawn. Moreover, the stereoscopic nature of this experiment compared to the two-component synthetic PIV simulations may reduce the commonality between them.

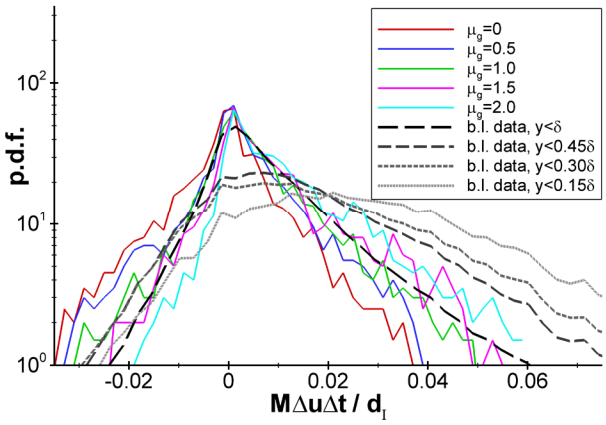

Fig. 11: Distribution of instantaneous velocity gradients du/dy in the boundary layer data. Also shown are the distributions from the synthetic PIV with shifting mean (σ_v=2.0, σ_g=2.0, and d_p=1.5).

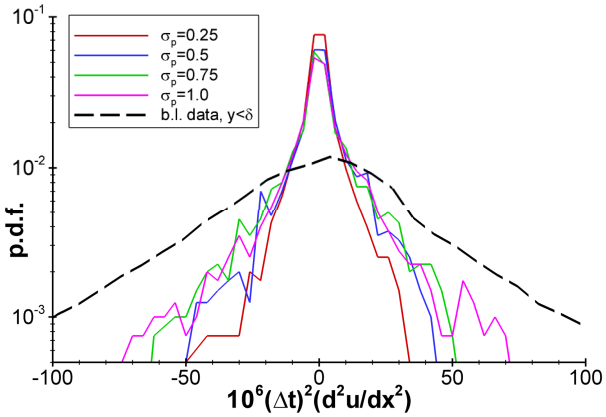

Fig. 12: Distribution of instantaneous second-order velocity gradients in the boundary layer data, d^2u/dy^2. Also shown are the distributions from the synthetic PIV (μ_g=0, σ_v=2.0, σ_g=2.0, and d_p=1.5).

Finally, Fig. 12 shows the distribution of second-order velocity gradients in the boundary layer, compared with those from the synthetic PIV. The largest second derivatives were found to be d^2u/dy^2, therefore these are shown in the figure. Their magnitude is considerably greater than those present in the synthetic PIV, and would suggest that considerable error may yet be found in both the IDT and LaVision interrogation of the data. It additionally would suggest that the spatial resolution of the experiment was inadequate to the gradients actually present in the flow. However, the apparent error in Fig. 10b is about half that predicted by the magnitude of the first-order velocity gradients, so further investigation is warranted before definitive conclusions may be drawn regarding the magnitude of errors due to second-order velocity gradients.

Conclusion and Future Work

The present investigation studies the error in Particle Image Velocimetry (PIV) interrogation due to the presence of velocity gradients in turbulent flows, for both classical and advanced algorithms. Classical algorithms are considered to be digital implementations of cross-correlation-based analysis with the incorporation of discrete window offsets. For the purposes of the present work, advanced algorithms are those using image deformation to compensate for the effects of velocity gradients. Synthetic PIV simulations of one-dimensional turbulence have shown that substantial biases in the turbulent stress towards lower values occur for classical algorithms even for velocity gradients that lie within the recommended PIV design limits. This bias error worsens if the probability distribution of velocity gradients in the flow has a nonzero mean, and in fact error in the mean velocity may be introduced as well. Advanced algorithms, on the other hand, do not exhibit this bias error if the velocity gradients are linear. Once nonlinear velocity gradients are examined, the error in the classical algorithm increases and a significant negative bias in the turbulent stress arises for the advanced algorithm as well.

Two experiments were interrogated using both a classical algorithm and an advanced algorithm, one a jet in crossflow and the other a boundary layer flow. Both showed substantially lower turbulent stresses for the classical algorithm as compared with the advanced algorithm, as predicted by the synthetic PIV. However, while the error found in the jet-in-crossflow data matched the prediction based on synthetic PIV, the error shown in the boundary layer measurements was about half the prediction. Probability distributions of the velocity gradients found in the two real data sets as compared to those from the synthetic PIV indicate that the simulations do not fully represent physical data. The veracity of the simulated turbulence will need to be improved to resolve the discrepancy between its prediction and the actual error evident in the boundary layer data. Nonetheless, these observations imply that turbulence data published prior to the advent of advanced algorithms may underreport the magnitude of turbulent stresses.

Within the range of parameters studied, it appears that advanced algorithms do not return significant errors so long as the velocity gradients may be considered reasonably linear. No new experimental design rules for advanced algorithms are yet proposed, but any such recommendation would concern second-order velocity derivatives rather than first order.

References

[1] Scarano, F., "Iterative Image Deformation Methods in PIV," *Measurement Science and Technology*, Vol. 13, No. 1, 2002, pp. R1-R19.

[2] Stanislas, M., Okamoto, K., Kahler, C. J., and Westerweel, J., "Main Results of the Second International PIV Challenege," *Experiments in Fluids*, Vol. 39, No. 2, 2005, pp. 170-191.

[3] Keane, R. D., and Adrian, R. J., "Theory of Cross-Correlation Analysis of PIV Images," *Applied Scientific Research*, Vol. 49, No. 3, 1992, pp. 191-215.

[4] Willert, C. E., and Gharib, M., "Digital Particle Image Velocimetry," *Experiments in Fluids*, Vol. 10, No. 4, 1991, pp. 181-193.

[5] Westerweel, J., Dabiri, D., and Gharib, M., "The Effect of a Discrete Window Offset on the Accuracy of Cross-Correlation Analysis of Digital PIV Recordings," *Experiments in Fluids*, Vol. 23, No. 1, 1997, pp. 20-28.

[6] Scarano, F., and Riethmuller, M. L., "Iterative Multigrid Approach in PIV Image Processing with Discrete Window Offset," *Experiments in Fluids*, Vol. 26, No. 6, 1999, pp. 513-523.

[7] Wieneke, B., "Stereo-PIV using Self-Calibration on Particle Images," *Experiments in Fluids*, Vol. 39, No. 2, 2005, pp. 267-280.

[8] Hart, D. P., "PIV Error Correction," *Experiments in Fluids*, Vol. 29, No. 1, 2000, pp. 13-22.

[9] Quenot, GM, Pakleza, J, Kowalewski, T. A., "Particle Image Velocimetry with Optical Flow," *Experiments in Fluids*, Vol. 25, No. 3, 1998, pp. 177-189.

[10] Beresh, S. J., "Evaluation of PIV Uncertainties using Multiple Configurations and Processing Techniques," AIAA Paper 2008-0239.

[11] Scarano, F., and Riethmuller, M. L., "Advances in Iterative Multigrid PIV Image processing," *Experiments in Fluids*, Vol. 29, No. 7, 2000, pp. S51-60.

[12] Huang, H. T., Fiedler, H. E., and Wang, J. J., "Limitation and Improvement of PIV, Part II: Particle Image Distortion, a Novel Technique," *Experiments in Fluids*, Vol. 15, No. 4-5, 1993, pp. 263-273.

[13] Lecuona, A., Nogueira, J., Rodriguez, P. A., and Acosta, A., "PIV Evaluation Algorithms for Industrial Applications," *Measurement Science and Technology*, Vol. 15, No. 6, 2004, pp. 1027-1038.

[14] Fincham, A., and Delerce, G., "Advanced Optimization of Correlation Imaging Velocimetry Algorithms," *Experiments in Fluids*, Vol. 29, No. 7, 2000, pp. S13-S22.

[15] Meunier, P., and Leweke, T., "Analysis and Treatment of Errors Due to High Velocity Gradients in Particle Image Velocimetry," *Experiments in Fluids*, Vol. 35, No. 5, 2003, pp. 408-421.

[16] Lecordier, B., and Trinité, M., "Advanced PIV Algorithms with Image Distortion Validation and Comparison using Synthetic Images of Turbulent Flow," *Particle Image Velocimetry: Recent Improvements: Proceedings of the EUROPIV2 Workshop*, 2004, pp. 115-132.

[17] Adrian, R. J., "Twenty Years of Particle Image Velocimetry," *Experiments in Fluids*, Vol. 39, No. 2, 2005, pp. 159-169.

[18] Stanislas, M., Okamoto, K., Kahler, C. J., Westerweel, J., and Scarano, F., "Main Results of the Third International PIV Challenge," *Experiments in Fluids*, forthcoming.

[19] Piirto, M., Eloranta, H., Saarenrinne, P., and Karvinen, R., "A Comparative Study of Five Different PIV Interrogation Algorithms," *Experiments in Fluids*, Vol. 39, No. 3, 2005, pp. 571-588.

[20] Keane, R. D., and Adrian, R. J., "Optimization of Particle Image Velocimeters. Part 1: Double Pulsed Systems," *Measurement Science and Technology*, Vol. 1, No. 11, 1990, pp. 1202-1215.

[21] Westerweel, J., "Fundamentals of Digital Particle Image Velocimetry," *Measurement Science and Technology*, Vol. 8, No. 12, 1997, pp. 1379-1392.

[22] Christensen, K. T., "The Influence of Peak-Locking Errors on Turbulence Statistics Computed from PIV Ensembles," *Experiments in Fluids*, Vol. 36, No. 3, 2004, pp. 484-497.

[23] Astarita, T., and Cardone, G., "Analysis of Interpolation Schemes for Image Deformation Methods in PIV," *Experiments in Fluids*, Vol. 38, No. 2, 2005, pp. 233-243.

[24] Kim, B. J., and Sung, H. J., "A Further Assessment of Interpolation Schemes for Window Deformation in PIV," *Experiments in Fluids*, Vol. 41, No. 3, 2006, pp. 499-511.

[25] Beresh, S. J., Henfling, J. F., Erven, R. J., and Spillers, R. W., "Penetration of a Transverse Supersonic Jet into a Subsonic Compressible Crossflow," *AIAA Journal*, Vol. 43, No. 2, 2005, pp. 379-389.

[26] Beresh, S. J., Henfling, J. F., Erven, R. J., and Spillers, R. W., "Turbulent Characteristics of a Transverse Supersonic Jet in a Subsonic Compressible Crossflow," *AIAA Journal*, Vol. 43, No. 11, 2005, pp. 2385-2394.

[27] Westerweel, J., "Theoretical Analysis of the Measurement Precision in Particle Image Velocimetry," *Experiments in Fluids*, Vol. 29, No. 7, 2000, pp. S3-S12.